Vertically polarized lasing and photoluminescence in crescent-shaped quantum wires

S Watanabe[1)], S Koshiba[2)], M Yoshita[1)], H Sakaki[3)], M Baba[1)], and H Akiyama[1)]

1) Institute for Solid State Physics, University of Tokyo.

2) Advanced Materials Science, Faculty of Engineering, Kagawa University.

3) Institute of Industrial Science, University of Tokyo.

Abstract. We studied polarization properties of a ridge quantum wire (QWR) laser structure. We optically excite the sample by mode-locked green laser, and measure polarization-dependent emission intensity from a cleaved facet of the structure. Interesting point is that the polarization of photoluminescence and lasing in the QWR is almost vertical to the potential, which is opposite to the results for other crescent-shaped quantum wire lasers. We theoretically show the mechanism for vertically-polarized transition via finite element calculations on the basis of 4x4 Luttinger Hamiltonian. We find that the different effective mass of electrons and holes, especially anisotropic effective mass of holes cause different shapes of wave functions, which results in greater oscillator strength of vertically-polarized transition.

1. Introduction

Crescent-shaped quantum wire (QWR) lasers without strain are considered to be polarized horizontally along their potentials[1,2]. However, inclined polarization of lasing was observed recently[3], and we also measured vertically polarized lasing in ridge QWR lasers. In this work, we study polarization properties of a ridge QWR laser structure and show that it lases in vertical polarization for excited state transition, and theoretically show the mechanism. We optically excite the sample, and measure polarization-dependent emission intensity from a cleaved facet of the sample. Interesting point is that the polarization of photoluminescence (PL) and lasing in the QWR is almost vertical to the potential, which is opposite to the results for other crescent-shaped quantum wire lasers[1,2]. We calculate the polarization-dependent transition matrix elements via finite element methods on the basis of 4x4 Luttinger Hamiltonian, and show the mechanism of the vertically-polarized transition.

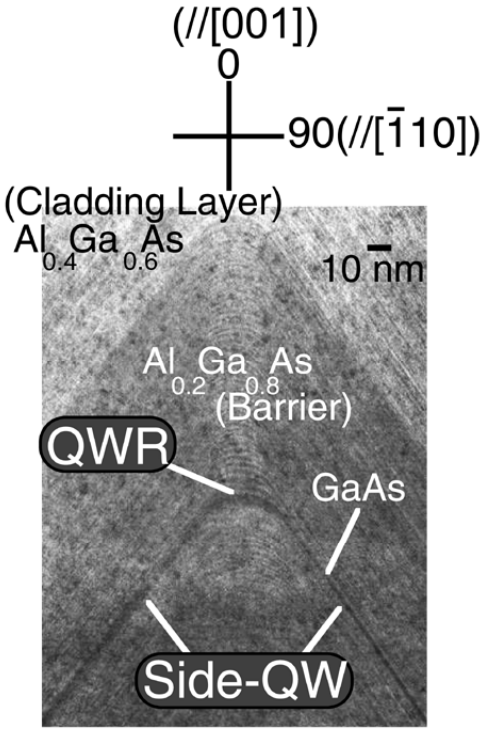

Figure 1. Cross-sectional TEM image of a ridge QWR laser structure.

2. Sample structure and experimental setup

The ridge QWR laser structure is formed via facet growth on a patterned substrate by molecular beam epitaxy[4]. A cross-sectional transmission electron microscope (TEM) image of the structure is shown in Fig. 1. A GaAs layer with a nominal vertical thickness of 5 nm is embedded in 90-nm thick barrier layers of a $Al_{0.2}Ga_{0.8}As$ digital alloy, which provides vertical confinement in the [001] direction. The layer of GaAs goes through a gradual curve at the top of the ridge structure, which provides lateral confinement along the GaAs layer. As a result, the QWR is formed at the ridge corner of the two [111]*B* adjacent quantum wells (QWs; here, side-QWs). The GaAs and $Al_{0.2}Ga_{0.8}As$ layers are sandwiched between the cladding layers of the $Al_{0.4}Ga_{0.6}As$ digital alloy, thus forming an optical waveguide structure. The sample was cleaved to form optical cavities of length L = 300 μm and the cleaved facets were left uncoated. As is shown in Fig. 1, we define θ =0 degrees as the direction of growth ([001] direction), and θ =90 degrees as the [$\bar{1}$10] direction.

Figure 2 shows a schematic of an experimental setup for the polarization measurement. We optically excite a sample by the second harmonics of continuous-wave mode-locked yttrium-lithium fluoride (YLF) laser pulses (526 nm, the repetition rate of 75.4 MHz, and the pulse duration of 50 ps). The pumping laser light was incident on the top of the ridge structure, and was focused by two cylindrical lenses (C.L.) into a stripe which uniformly covered the whole ridge QWR structure. Emissions from a cleaved facet were collected by an objective lens, passed through a Glan-Thompson polarizer (Pol.) , and were led to a monochromator. In order to monitor a position of excitation and observation, we illuminated the cleaved facet by a tungsten lamp (W-lamp), and observed a reflection image by a CCD camera. We should carefully consider the polarization dependence of

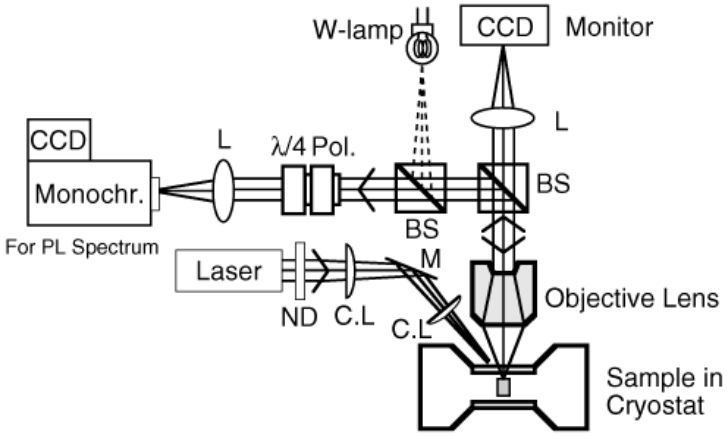

Figure 2. Schematic of an experimental setup for a polarization measurement. Notations and explanations of optical equipments are shown in the main text.

the optical equipments in the setup, since the polarization measurement is very sensitive to them. We chose the optical equipments to attenuate the polarization dependence of the experimental setup. We used beam splitters (BS) as "broadband non-polarizing hybrid cube beamsplitter" [Newport product number: 10BC17MB.2]. We put λ/4 waveplate (Achromatic Zero-Order Waveplate [Newport product number: 10RP44-2(3)]) after the polarizer to attenuate polarization dependence of the monochromator. In Sec. 3.2, we measured polarization-dependent spatial emission patterns from the cleaved facet. In this case, we put a CCD camera instead of the monochromator, and chose a detection wavelength by an interference filter[5].

3. Polarization measurements for a ridge quantum wire laser structure

3.1. Photoluminescence spectra and origin of emissions

Figure 3 shows the PL spectra from the cleaved facet of the ridge QWR laser structure with low excitation power (2 W/cm^2) at T = 4.5 K. The solid and dashed lines represent

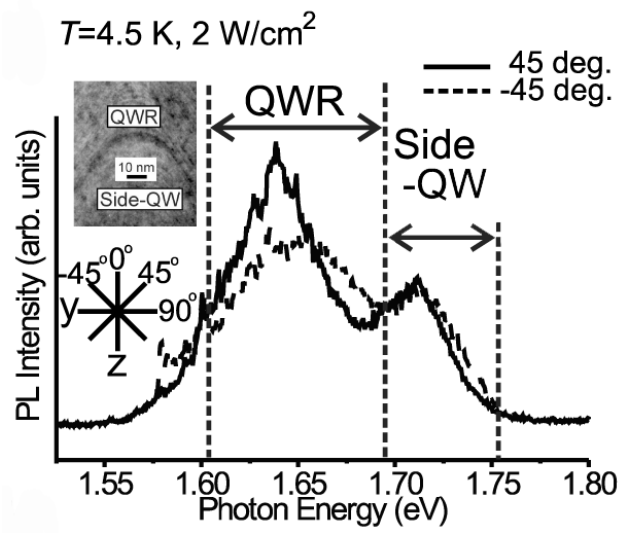

Figure 3. PL spectra from a cleaved facet of a ridge QWR laser structure with low excitation power (2 W/cm^2) at T = 4.5 K. The solid and dashed lines represent the PL spectra at the polarization of 45 (solid) and –45 (dashed) degrees.

the PL spectra at the polarization of 45 (solid) and –45 (dashed) degrees. Emission from the Side-QWs and the QWRs is observed, the respective origins were confirmed by photoluminescence (PL) imaging measurements[6].

3.2. Polarization measurement for adjacent side-quantum wells

Figure 4 shows the polarization dependent PL patterns from side-QWs. An image at the top of Fig. 4 shows a PL emission pattern from the cleaved facet at 1.703 eV of photon energy without polarizer. The PL image follows the geometry of side-QWs. Two images of the lowest part show the PL patterns at the same photon energy with polarizer parallel to two side-QW directions. The polarizer clearly separates the emission pattern of the right and left parts of the side-QW structures. The optical transition between electrons and heavy holes in the QW structures is polarized parallel to the potential layers, which cause the separation of PL patterns.

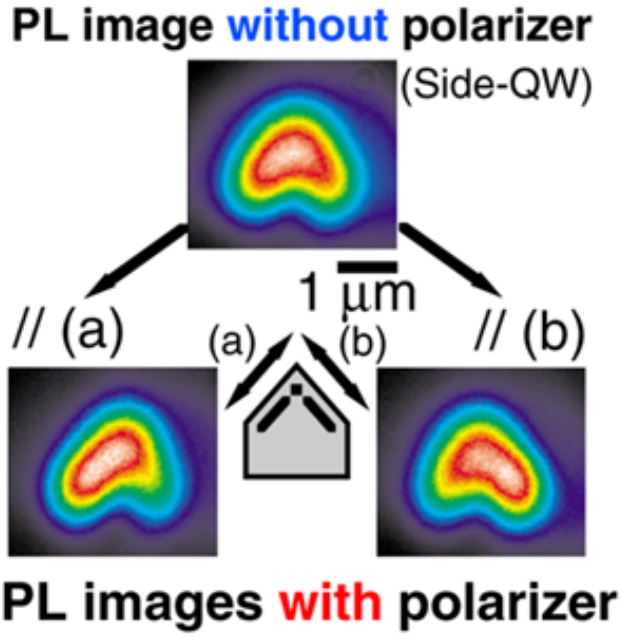

Figure 4. Spatially and spectrally resolved emission patterns of the side-QWs (at 1.703 eV) from the cleaved facet at T = 4.5 K. (Top) Emission pattern without polarizer. (Bottom) Emission patterns with polarizer parallel to two side-QW directions.

3.3. Polarization measurement for a ridge quantum wire

Figures 5 (a)-(c) show the excitation power dependence of emission spectra at T = 4.5 K. Emission from the side-QWs and the QWR is observed in Fig. 5(a). As the amount of power is increased to obtain Fig. 5(b), the spectral peak is blueshifted due to state-filling; this process continues until finally, in Fig. 5(c), lasing has occurred at the interband transition between higher-order excited states.

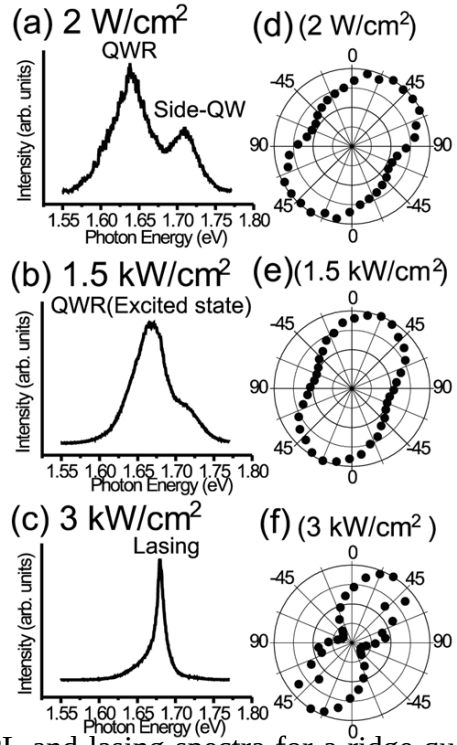

Figure 5. (a)-(c) PL and lasing spectra for a ridge quantum-wire laser at T = 4.5 K for levels of excitation power of (a) 2 W/cm^2, (b) 1.5 kW/cm^2, and (c) 3 kW/cm^2. (d)-(f) Polar plots of polarization for the spectral peak from a cleaved edge plane of the QWR in the three states of Fig. 2(a)-(c). Both PL and lasing have a pronounced vertical polarization. Lasing is linearly polarized.

Figures 5 (d)-(f) show the polarization dependence of emission intensity at each of the energy-spectral peaks for the QWR in (a)-(c). The definition of the polarization angles is shown in Fig. 1. Each of the patterns shows a pronounced vertical polarization. At the low level of excitation power shown in Fig. 5(d), spontaneous emission from the QWR is polarized to 45 degrees. As we increase the level of excitation power to reach the situation of Fig. 5(e), the emission becomes polarized to 20 degrees. Stimulated emission is linearly polarized to 35 degrees in Fig. 5(f).

4. Numerical calculation of the polarization dependence of oscillator strength for a ridge quantum wire structure

4.1. Numerical method

We next compute polarization-angle dependent oscillator strength for the ground- and excited-state transitions, to explain the vertically-polarized spontaneous and stimulated emissions. We use the 4x4 Luttinger Hamiltonian[7] as the basis for numerical calculation of the wave functions of electrons and holes for the potential shown in Fig. 1, and compute polarization-angle-dependent transition matrix elements. We apply the finite element methods with 8720 right-triangular elements to numerically calculate approximate solutions to the Schrödinger equations for the electrons and holes. The details of the method of calculation are given in a separate article[8].

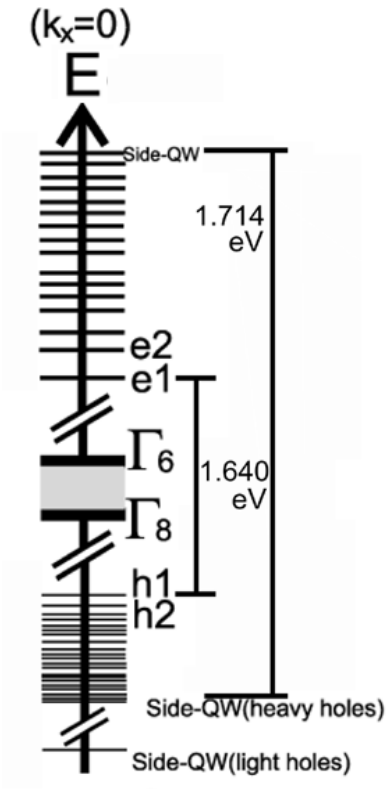

Figure 6. Energy levels of confined eigenstates at the band edge for the electrons and holes

The energy levels of the confined eigenstates at the band edge for the electrons and holes are shown in Fig. 6. There are 15 confined states for electrons and 20 confined states for holes. The calculated energies of the ground state transition of QWRs (e1-h1 transition) and side-QWs are 1.640 eV and 1.714 eV respectively, which is good agreement with the PL photon energy in Fig. 3.

4.2. Polarization dependence of oscillator strength

Figure 7 shows calculated squares of the oscillator strength for ground- and excited-state transitions. The polarization axis for the e1-h1, e2-h2, e3-h3, and e4-h4 [e(n)-h(n)] transition is almost horizontal while, for the e2-h1, e3-h2, e4-h3, and e5-h4 [e(n+1)-h(n)] transitions, it is almost vertical. The results of calculation reveal that the vertically-polarized transitions (e(n+1)-h(n)) have much greater oscillator strengths, and this provides a good explanation of our results in Fig. 5.

4.3. Wavefunctions of electrons and holes

Next, we explain why our calculation produced a much greater oscillator strength for the e(n+1)-h(n) transition than for the e(n)-h(n) transition. Figure 8 is a set of contour plots of the squares of the wave functions for electrons (e1, e2, ...) and holes (h1, h2, ...), as obtained by the numerical calculation. The quantization energy of each state is also shown. For both electrons and holes, the number of nodes in the wave functions increases in a one to one correspondence with increases in the quantum number.

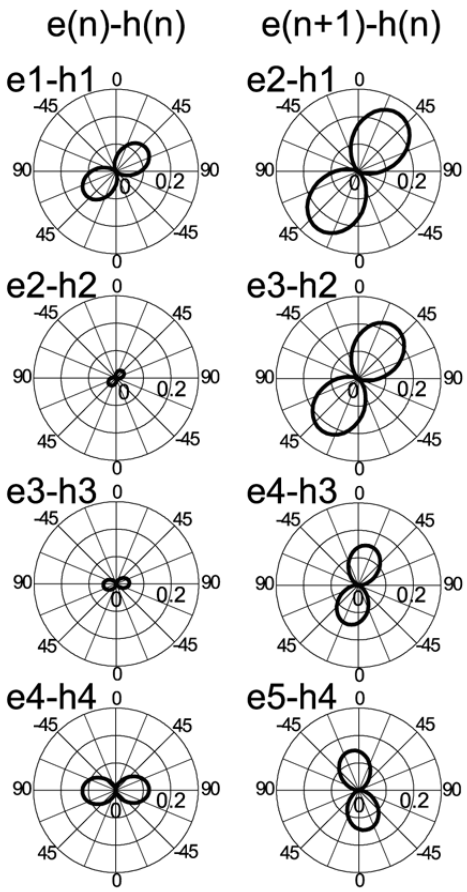

Figure 7. Calculated squares of the oscillator strength for ground- and excited-state transitions. The polarization axis for the e1-h1, e2-h2, e3-h3, and e4-h4 [e(n)-h(n)] transition is almost horizontal while, for the e2-h1, e3-h2, e4-h3, and e5-h4 [e(n+1)-h(n)] transitions, it is almost vertical and their oscillator strength is large.

Note that the wave functions of the holes spread further into the side-QW regions than those for electrons that have the same quantum number. This is because the effective mass of the electrons is light and isotropic, while that of the holes is heavy and anisotropic. The effective mass of holes are anisotropic, and the mass toward [111] direction in the Side-QW regions is heavier than that toward [001] direction in the QWR region. This leads to a smaller difference between the quantization energy of the side-QWs and the QWR than the electrons. Thus, the holes have a much weaker lateral confinement than the electrons, which is why the wave functions of the holes spread further into the side-QW regions.

Note that the positions of maximum probability density for a h(n) state are almost the same as those for the corresponding e(n+1) state due to the different confinement potentials for electrons and holes. Oscillator strength is determined by the overlap integrals of the envelope functions of electrons and holes. The greater oscillator strength for the e(n+1)-h(n) transitions in our calculation was derived from the same position of maximum probability density for the e(n+1) and h(n) states.

5. Conclusions

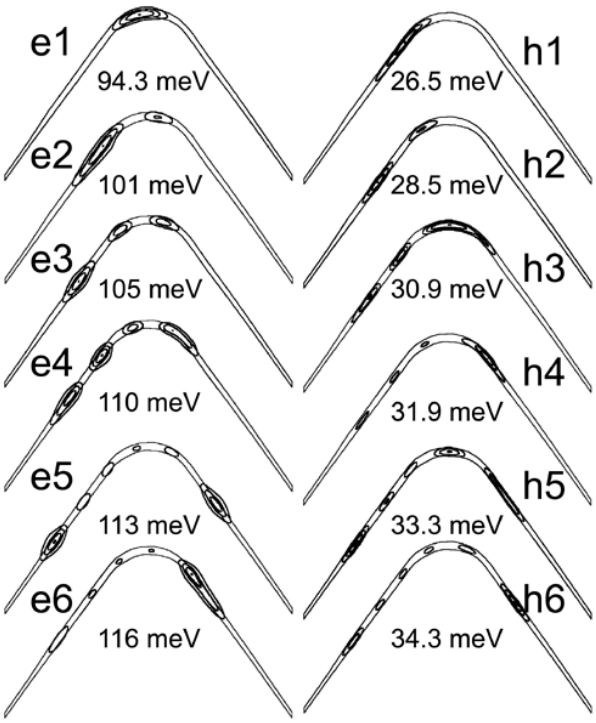

Figure 8. Set of contour plots of the squares of the wave functions for electrons (e1, e2, ...) and holes (h1, h2, ...), as obtained by the numerical calculation. The quantization energy of each state is also shown.

In this article, we studied polarization properties of a ridge quantum wire (QWR) laser structure. The polarization of PL and lasing in the ridge QWR is almost vertical to the potential. We numerically calculate the wave functions of electrons and holes and theoretically show the mechanism for vertically-polarized transition. We find that the different effective mass of electrons and holes, especially anisotropic effective mass of holes cause different shapes of wave functions, which results in larger oscillator strength for vertically-polarized transition.

Acknowledgement: The Ministry of Education, Culture, Sports, Science and Technology, Japan provided a Grant-in-Aid that helped us to complete this work. One of the authors (S.W.) must also thank the Japan Society for the Promotion of Science (JSPS) for the financial support the society provided.

References

[1] T. G. Kim *et al.*, Physica E **7**, 508 (2000).
[2] L. Sirigu *et al.*, Physica E **7**, 513(2000).
[3]C. Percival *et al.*, Appl. Phys. Lett. **77**, 2967 (2000).
[4] S. Koshiba *et al.*, J. Crystal Growth , **201/202**, 810 (1999).
[5] M. Yoshita *et al.*, J. Appl. Phys., **83**, 3777 (1998).
[6] S. Watanabe *et al.*, Appl. Phys. Lett., **73**, 511 (1998).
[7] J. M. Luttinger, and W. Kohn, Phys. Rev., **97**, 869 (1955).
[8] S. Watanabe *et al.*, to be published in Jpn. J. Appl. Phys.